The Optical Spectropluviometer Revisited

CHRISTIAN SALLES

Geofluides Bassins Eau, Université de Montpellier, Montpellier, France

JEAN-DOMINIQUE CREUTIN

Laboratoire d'Etude des Trauferts en Hydrologie et Environnement, Université de Grenoble, Grenoble, France

DANIEL SEMPERE-TORRES

Deparamento d'Enginyeria Hydràulica, Maritima i Ambiental, Universitat Politecnica de Catalunya, Barcelona, Spain

21 February 1997 and 1 October 1997

ABSTRACT

The optical spectropluviometer is a shadowgraph instrument able to measure independently the equivalent diameter and the fall speed of raindrops at ground level. Hardware and software modifications are proposed and tested. A modern digital signal processing system allows for the simultaneous sampling and analyzing of the signal delivered by the sensor. The IR light transmission is pulsed to avoid interference with natural radiation and the protection of the optics is improved. The validation procedure consists of comparing the rain rates derived from the measured drop size distributions with rain rates delivered by nearby rain gauges. The results obtained during 65 storm events show that the proposed improvements reduce the bias of the rain-rate estimation from 34% to 16%. Suggestions are given to further improve the performance of this instrument.

1. Introduction

The optical spectropluviometer (OSP) was designed to measure automatically the size and fall velocity distributions of raindrops at ground level. Introduced by Picca and Trouilhet (1964), the principle of this shadowgraph instrument is simple. The IR light (0.9-μm wavelength) transmitted by a diode (LED) is shaped into a 100-cm^3 cuboid beam of parallel light by a pair of converging lenses and rectangular masks. The total light intensity transmitted through the beam is monitored by a single receiving photodiode that delivers an electric signal proportional to the received light intensity. When a particle falls across the beam, the light intensity received by the photodiode decreases. The amplitude and the duration of the signal variation are proportional to the cross section of the particle and to its residence time in the beam, respectively. The residence time can be converted to a fall speed, assuming the particle crosses the two horizontal faces of the beam (separated by a known height of 1 cm).

Corresponding author address: Christian Salles, Laboratory for Experimental Geomorphology, Redingenstraat 16, B-3000 Leuven, Belgium.
E-mail: christian.salles@geo.kuleuven.ac.be

The OSP was first developed and tested by Donnadieu et al. (1969). The signal processing used at that time delivered only the size and fall speed spectra, and it turned out to be impossible to assign a size and a speed to each individual drop. Improvements of the processing system allowed Donnadieu (1974, 1978, 1980) to compare the OSP measurements with those of a Joss–Waldvogel disdrometer and to measure drop fall velocities in rain different from the Gunn and Kinzer results in still air. Both the sensor and the processing system of the OSP were redesigned by Klaus (1977) and then by Hauser et al. (1984, Hauser hereafter). The working principle has remained unchanged and simple compared to other shadowgraph instruments like the particle measuring system, using a linear array of 64 photodiodes (Knollenberg 1970, 1976); or the optical rain gauge, working on a scintillation principle (Wang et al. 1979); or the paired-pulsed optical disdrometer, whose beam is a cylindrical sheath of light (Illingworth and Stevens 1987). Notwithstanding its simplicity, this principle offers several advantages. The electronics and the optics of the sensor are not sophisticated, so it makes the instrument easy to calibrate, and it is reliable and robust. The delivered signal is not difficult to process continuously. The drop counts can be expressed either in terms of fluxes through the 100 cm^2 horizontal surface of the

beam or in terms of concentrations. The concentration is inversely proportional to the beam volume and proportional to the ratio of the sum of the residence times of the drops in the considered diameter range to the total sample time.

According to Hauser, the OSP suffers from different problems. In addition to the sampling uncertainties, common to all the above-mentioned sensors, the two major sources of error were reported to be the signal processing used and the environmental conditions. The objective of the present work is to address some of these errors via a complete overhaul of the signal processing system and some minor hardware modifications (use of pulsed IR signal and increased protection of the optics). Given the difficulty in choosing a reference instrument and appropriate criteria to control the obtained size and fall speed spectra, it was decided to concentrate on rain-rate estimates. Of course this bulk variable is not uniquely related to the size spectrum. However, if derived bulk variables are systematically different from those measured with classic gauges, the measured spectra are unsatisfactory. In addition, the direct collection of rainwater volume by gauges provides an undeniable means to check indirect estimates even if the gauges themselves are not free of errors (see Rodda 1967). As the OSP directly measures the flux through horizontal surface, the proposed validation does not depend on the measured fall speed spectrum.

In section 2 the instrument modifications are presented. Section 3 describes the experimental setup and the resulting analysis showing the effect of these modifications. In section 4 unsolved issues are discussed and some conclusions are drawn.

2. Sensor modifications and calibration

a. Digital signal processing

The electronic receiver of the sensor was kept unchanged. It suppresses the DC component and inverts, amplifies, and takes the square root of the signal delivered by the receiving photodiode.

In Hauser's version, an analog signal processing module extracted the peak and the integral of the signal pulse. The peak value determined the diameter of the particle. The residence time was derived from both the peak value and the integral (see section 2 of Hauser). This type of processing suffers essentially from its inability to analyze the signal resulting from the presence of more than one drop in the beam and from the undesirable link between the size and the speed computations. Those problems were mitigated by rejecting the drops with an ''anomalous'' size–speed ratio compared to a theoretical relationship.

A modern digital acquisition processor (DAP) implemented on a microcomputer has been substituted for the analog module. The multitask capability of this processor allows simultaneous sampling and real-time processing of the signal, avoiding any kind of dead time.

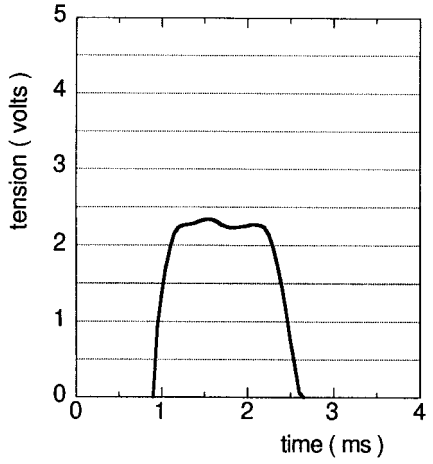

(a) D = 2.3 mm, V = 7.7 m s^{-1}

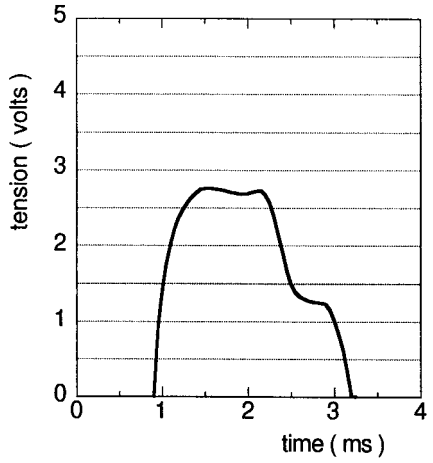

(b) D = 2.4 mm, V = 7.7 m s^{-1} and D = 1.2 mm, V = 5.0 m s^{-1}

FIG. 1. Examples of raindrop signals captured in real conditions and assumed to result from (a) one and (b) two drops passing the light beam. The DAP identified diameter (D in mm) and fall velocity (V in m s^{-1}) are indicated below each picture.

For test purposes, the DAP signal processing was first designed to mimic the analog module algorithm. Later, the signal processing was completely redesigned to take advantage of the shape recognition capabilities of the digital system. A 10-kHz sample rate was chosen to obtain a good description of the fastest drops (see, e.g., Fig. 1—the flat parts of the signal are defined by at least 10 points). The continuous recording and analysis of both the level and the slope of the signal by the DAP allows recognition of the entrance (positive slope), the presence (nil slope and level above noise), and the exit (negative slope) of each drop in the beam. When two drops are simultaneously present (see Fig. 1), the di-

ameter identification of the drops depends on the modification of the slope changes and on the combination of the extinction levels. For each drop, the diameter [corrected for the oblate ellipsoid effect according to Pruppacher and Pitter (1971)], the residence time and the arrival time (the time of the positive slope outbreak, i.e., the entrance of the drop) are computed and archived on a hard disk (1 megabyte allows the storage of 1.5 h of rain measurement). In the case of unrecognized signal waveforms (in particular when more than two drops are simultaneously present in the beam) an error flag was generated, dated, and stored.

b. Pulsed transmission

The OSP has been known to be sensitive to solar IR radiation. In daylight conditions the diameters of calibrated spheres were underestimated on average by 6% compared to night conditions. This is simply due to the fact that in daytime conditions the drops intercept a smaller proportion of the IR light reaching the receiver; the solar radiation was constant.

The continuous transmitting mode of the IR light source (LED) was converted to a pulsating mode with a 1-μs pulse each 64 μs. Simultaneously, the sample and hold at the output of the receiving photodiode was doubled in order to be able to capture both the LED signal (during the pulse) and the environmental signal (between two pulses). The difference between the two sampled signals was used to identify the drops.

These modifications, proposed and implemented by the Centre d'Études de l'Environnement Terrestre et Planétaire (the laboratory at the origin of the OSP development), give essentially two advantages over the continuous transmission device. First, the instantaneous energy transmitted by the LED is multiplied by a factor of 10 and thus the level of the useful signal is dramatically increased compared to the natural IR radiation. In addition, the doubled signal sampling gives the opportunity to completely eliminate the natural component from the processed signal.

c. Splash protection

Under wind conditions, raindrops are able to penetrate the optics protection, to produce small splash droplets on the lenses themselves, and thus to create optical heterogenities. The presence of such small droplets was visually confirmed by inspecting the sensor shortly after different storms.

Simple visors were added to the existing protecting covers of the transmitter and the receiver. First, this setup prevents direct drop impacts on and dripping along the protecting covers. In addition, as the visors are close to the beam (less than 1 cm), the shadow effect of the transmitter and receiver boxes, due to the wind component parallel to the beam axis, is reduced significantly. For instance, with a 10 m s^{-1} wind speed parallel to the beam and assuming a Marshall–Palmer drop size distribution, the rain-rate underestimation theoretically decreases from 25% to 11% for a 20 mm h^{-1} rain rate (see the appendix). This modification also reduces the sampling surface by 40%. This results both in an increase of the sampling fluctuations and in a decrease of the multiple drop probability. For instance, if we assume a rain rate equal to 40 mm h^{-1} and a Marshall–Palmer drop size distribution, and if we use the Poisson computation of Stow and Jones (1981), the probability of having only one drop at the same time in the beam increases from 83% to 89% when the sampling surface is reduced from 100 to 60 cm^2.

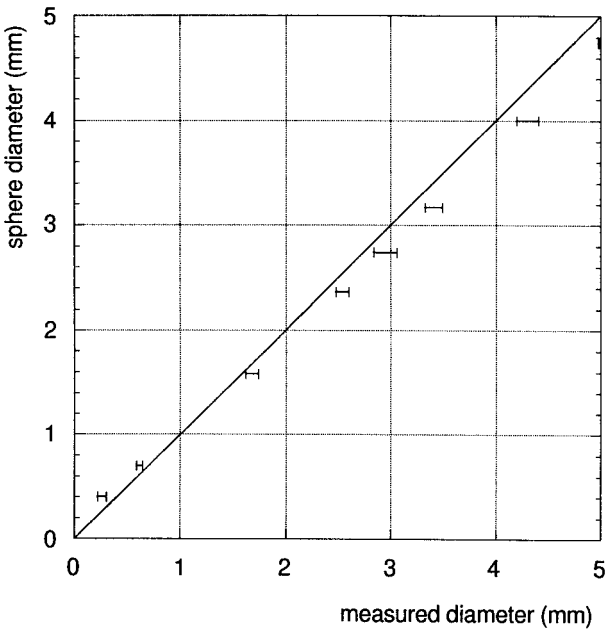

FIG. 2. Relationship between the measured diameter and the actual diameter for six different sizes of steel spheres and two different sizes of water drops. The smallest drops (0.4 mm in diameter) were produced by a fine capillary connected to a vibrating membrane. The largest ones (3.5 mm) were obtained with a hypodermic needle. The horizontal bars cover the range of measured diameters, depending on the location where the test particles are passing the light beam.

d. Indoor calibration

The sensor is designed to deliver a voltage of 1 V for a particle diameter equal to 1 mm. Overestimation and underestimation of, respectively, the larger and the smaller diameters are expected from diffraction effects. The complete measurement range was calibrated by using steel and glass spheres of different sizes and water drops. Figure 2 summarizes the obtained results, leading to a linear correction of the type

$$D^* \text{ (mm)} = 0.911 D_m \text{ (mm)} + 0.11, \qquad (1)$$

where D_m is the delivered value and D^* is the corrected one. The measurements are found not to depend on the nature of the sphere but on its location in the beam.

Across the beam the apparent diameters systematically decrease by 5% to 10% close to the vertical edges. This nonuniformity of the power radiated in the beam is apparently higher than the 3% found by Hauser. Longitudinal fluctuations are of the same order and depend on the particle size (see Fig. 2).

The stability of the sensors in time was tested by throwing a calibrated sphere (4 mm in diameter) several times at a given point in the beam. The maximum difference in the measured diameters was 6×10^{-2} mm and the obtained signals were in all cases very close to the theoretically expected shapes. The capacity of the acquisition system to capture high particle arrival rates was established using a turning transparent disk bearing opaque dots. The maximum number of dots that could be sampled and processed during 1 min was tested to be near 3000 in continuous mode and 5000 during a limited 5-min sample.

3. Validation results

a. The experimental setup

From March 1991 to October 1993 a set of ground rain sensors was tested in Grenoble and Marseille, France. This set included four types of tipping-bucket rain gauges (with sampling surfaces of 200, 400, 1000, and 2000 cm^2), a classic Joss–Waldwogel (1967) disdrometer (not used in this study), and two OSPs.

To distinguish the different tested versions, abbreviations are used. OSP1 designates the original hardware coupled with a processing algorithm mimicking the Hauser analog processing module, OSP2 is the same hardware coupled with the new signal processing algorithm, and OSP3 includes the pulsed signal and increased optics protection.

From March to June 1991, OSP1 was operated together with four tipping-bucket rain gauges in Grenoble, France, in a 1ow-altitude Alpine climate. During this period, 17 storms occurred, yielding a total rainfall depth of 135 mm and a maximum intensity of 19 mm h^{-1} in 6 min. The maximum mean difference between any pair of the four rain gauge readings was less than 5%, and the maximum mean difference from the gauge with the largest rim, which seems to be the most reliable one, was less than 3% (see Vastel 1991). From March to July 1992, OSP2 was tested in the same experimental context. The set of observations counts 30 storms totaling 223 mm with a maximum intensity of 36 mm h^{-1} in 6 min. Finally, from October 1992 to October 1993, the fully modified version OSP3 was operated in Marseille, France, in a Mediterranean climate. The 18 storms included in the database add up to 183 mm with a maximum intensity of 50 mm h^{-1} in 6 min.

Due to the particular emphasis put on the rain rate as a validation variable, the tipping-bucket rain gauges were regularly calibrated using a controlled inflow and the catch was weighed after each storm to check the coherence with the number of bucket tips. The observed differences were less than 6%. The weight corresponding to a bucket tip has been corrected according to the ratio between the weighted catch and the number of bucket tips during each rainy event.

b. Results

As shown in Fig. 3a, OSP1 gives, on average, rain rates that are systematically lower than the gauge measurements, and this underestimation nonlinearly depends on rain rate. According to the slope of the least squares fit straight line (0.66), the bias is 34%. A sharp break in the slope of the experimental scattergram appears around 7 mm h^{-1}, and for the higher rain rates the bias is about 50%. In spite of this nonlinearity the correlation coefficient is high (the determination coefficient obtained from 1177 points is 0.86). These underestimations typically took place in a storm sequence as follows. OSP1 captured well the beginning of the storm and correctly detected the first intensities lower than 7–8 mm h^{-1}. However, it fell behind when the intensities were higher. The acquisition software indicated more than 50% of signal rejections.

The OSP1 results reported here are in agreement with the limited set of published diagrams and numbers about this shadowgraph. The VIDIAZ instrument of Donnadieu (1980) gave a 44% underestimation compared to a Joss–Waldvogel disdrometer, and the OSP of Hauser was reported to yield a 27% underestimation (for a 2-min integration period) for rain rates over 10 mm h^{-1}.

Figure 3b depicts the corresponding results similarly obtained with OSP2. The slope of the regression line (0.79) indicates a significant reduction of the bias to 21%. The determination coefficient is equal to 0.91 (obtained from 3493 points). The improvement obtained over the original analog signal processing module is thus appreciable, but large discrepancies still occur for the three rain rates observed over 15 mm h^{-1}.

According to Fig. 3c, the hardware improvements leading to OSP3 again improved the comparison. The slope of the regression line (0.84) indicates less than 16% bias and the determination coefficient is 0.94 (1236 points). It must also be noted that the behavior is almost linear over the range from 0 to 40 mm h^{-1}; only the highest point seems to be in contradiction with this linearity.

4. Unsolved issues and concluding remarks

Apart from these positive results, the question is: What is the origin of the remaining 16% underestimation? At least two major potential causes can be mentioned.

1) The wind effect is certainly a significant cause. In the absence of wind data (a lack in the experimental design), a theoretical computation can give an idea of the wind effect on rain-rate measurement (see appen-

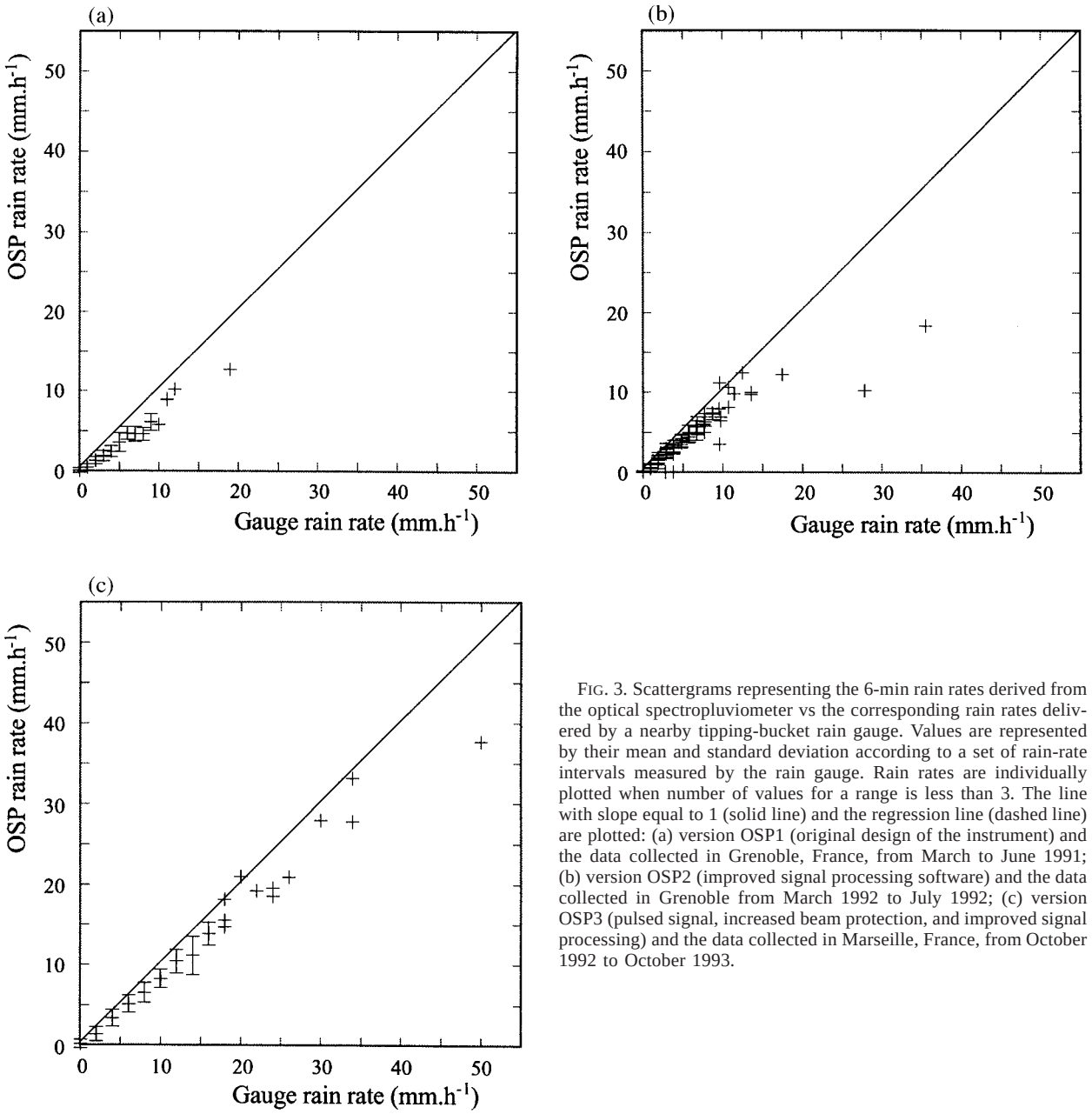

FIG. 3. Scattergrams representing the 6-min rain rates derived from the optical spectropluviometer vs the corresponding rain rates delivered by a nearby tipping-bucket rain gauge. Values are represented by their mean and standard deviation according to a set of rain-rate intervals measured by the rain gauge. Rain rates are individually plotted when number of values for a range is less than 3. The line with slope equal to 1 (solid line) and the regression line (dashed line) are plotted: (a) version OSP1 (original design of the instrument) and the data collected in Grenoble, France, from March to June 1991; (b) version OSP2 (improved signal processing software) and the data collected in Grenoble from March 1992 to July 1992; (c) version OSP3 (pulsed signal, increased beam protection, and improved signal processing) and the data collected in Marseille, France, from October 1992 to October 1993.

dix). The drops are assumed to fall at their terminal fall velocities in still air (Beard 1976) and to horizontally follow the wind. Figure 4 gives the relative error in the rain-rate estimate resulting from a 10 m s^{-1} horizontal wind blowing either parallel or perpendicular to the optical beam axis under two different drop size distribution types [Marshall–Palmer (1948) or gamma]. For rain intensities over 20 mm h^{-1}, the relative error is negative (underestimation) and ranges are from -10% to -15%, depending on the direction of the wind and the rain rate. These results must be considered with care since the OSP structure certainly modifies the wind field around the beam. The use of a small-scale model of the OSP in a water channel provided confirmation that the created turbulent field significantly modifies the drop trajectories (the drops were simulated by calibrated bubbles). This comment particularly applies to low rain intensities with essentially small drops that are very sensitive to this small-scale turbulence. Note that, for the same reasons, wind is also known to induce systematic rain gauge underestimations. However, according to the published results about short time steps and high intensities, the catch deficit does not a priori reach more than 10% for 10–20 m s^{-1} winds (Folland 1988).

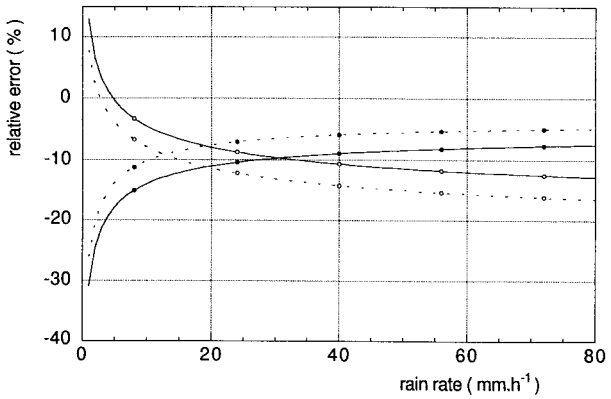

FIG. 4. Theoretical relative error in the rain-rate estimate as a function of the rain rate. A 10 m s^{-1} wind is considered to blow either parallel (black dots) or perpendicular (empty dots) to the optical beam axis. The drops are supposed to be distributed in size either according to a Marshall–Palmer (solid lines) or gamma (dashed lines) formulation.

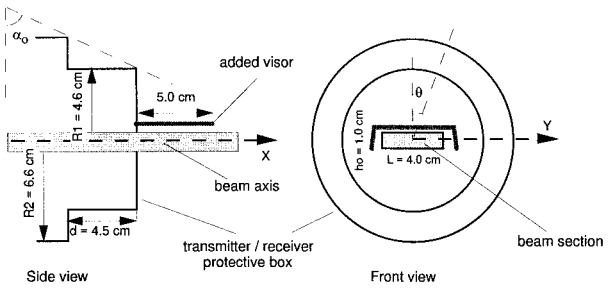

FIG. A1. Detailed views of the transmitter/receiver protective box (the x axis is chosen parallel to the beam, the y axis perpendicular to the beam, and the angles α_0 and θ are used to compute the shadowed surface).

2) The limited range of measured diameters can be a second cause of underestimation. Given the electronic design, the theoretical range is from 0.2 to 5.0 mm. According to the correction relationship (1), the maximum measurable diameter is thus 4.7 mm (this corresponds to a maximum measurable cross section of 17.35 mm^2). This is a common feature since, for instance, both the Joss–Waldvogel disdrometer and the optical disdrometer by Illingworth and Stevens (1987) are limited to 5.0 mm. During high rain rates, the probability is not negligible to have one or several drops in the beam whose total cross-section area exceeds the limit. Assuming a rain rate equal to 100 mm h^{-1} and an exponential drop size distribution, Ulbrich (1985) found that a 0.8–5.0-mm truncation leads to a maximum of 5% underestimation (this result does not take into account the case of multiple drops in the beam with a total cross section exceeding the limit of 17.35 mm^2). The maximum measurable diameter has been recently extended to 7 mm in order to use the OSP under artificial rain produced by irrigation guns (see Augier 1997). This modification slightly improved the water volume assessment under this type of rain.

In conclusion the following recommendations can be made.

1) If some additional minor modifications are made to the sensor (extension of the detection range, multiple drop processing improvement), the wind effect will remain the only major and almost unresolvable source of uncertainty on OSP measurements. The use of a shielding device is recommended (the octagonal vertical double fence shield designated for the World Meteorological Organization gauge intercomparison should be tested).

2) The comparison with a rain gauge is a reliable first-order means to appreciate the improvements of a raindrop size measurement instrument. But, as far as the drop size distribution is concerned, it is likely that additional sources of uncertainty will remain that are hidden in the rain-rate comparison. For instance, depending on where the drop crosses the beam, the uncertainty in the measured diameter can be as high as 10% (see Fig. 2).

3) In this reconsideration of the OSP, only a very limited part of the possibilities of the instrument has been considered. Additional parameters, like the arrival time, the residence time, and the fall velocity, have to be analyzed as well.

Acknowledgments. This OSP study would not have been possible without the help of the Centre d'Étude de l'Environnement Terrestre et Planétaire in Paris, a CNRS (and formerly CNRS-CNET) laboratory that developed and improved the OSP; the Division Technique d'Electricité de France in Grenoble; the Société d'Exploitation du Réseau d'Assainisssement de Marseille that operated the rain gauges in Grenoble and Marseille, respectively; and the Laboratoire d'Étude des Ecoulements Géophysiques et Industriels, Grenoble, which contributed to some laboratory tests. F. Baudin, A. Cartellier, M. Queaux, C. Lallement, D. Laplace, and J. P. Vinson are warmly acknowledged for their respective contributions. The Services Techniques of the city of Marseille and the European Environment Programme gave the financial support for this study. Thanks are also due to the Service Commun d'Enseignement des Langues from the Université Montpellier II for English corrections and to the anonymous reviewers for their discerning recommendations.

APPENDIX

Wind Effects on Rain Measurement

The wind effect on raindrop trajectories modifies the OSP sampling surface. In the following computations, the raindrops are assumed to fall at their terminal fall velocities in still air (Beard 1976) and to horizontally follow the wind. The OSP structure is thus supposed to have only a minor impact on the wind field itself. The tilt angle α of a drop trajectory depends on the horizontal wind speed V_w and vertical fall velocity $V_t(D)$ according to

$$\tan\alpha = \frac{V_w}{V_t(D)}. \quad \text{(A1)}$$

The horizontal wind is considered either parallel or perpendicular to the light beam axis.

a. Wind parallel to the beam

Figure A1 gives a detailed views of the protective box (the transmitter and the receiver have identical protections). The box consists of two cylinders with radius R_1 (4.6 cm) and R_2 (6.6 cm), and the protective visor added on OSP3 is less than 1 cm from the beam.

When the wind blows parallel to the optical axis, the structure of the OSP intercepts drop trajectories shadowing a part of the sampling surface. If the y axis is chosen perpendicular to the optical beam x (see Fig. A1) and if L is the width of the beam, the detection range along y is between $-L/2$ and $L/2$. For a drop trajectory inclination angle α, the protective box will intercept the drops with potential impact coordinates (x, y) on the top of the beam if x is less than

$$x_s(y) = \tan\alpha(\sqrt{R_1^2 - y^2} - h_0/2), \quad \text{(A2)}$$

where $x_s(y)$ represents the border of the shadowed surface S_m given by the following integral:

$$S_m = 2\int_0^{L/2} x_s(y)\, dy. \quad \text{(A3)}$$

Using the angle θ as a new variable (see Fig. A1), x and y can be expressed as

$$x = (R_1\cos\theta - h_0/2)\tan\alpha \quad \text{and} \quad y = R_1\sin\theta.$$

The surface S_m becomes

$$S_m = 2\int_0^{\theta_m}\left\{R_1\cos\theta - \frac{h_0}{2}\right\} tg\alpha R_1\cos\theta\, d\theta, \quad \text{(A4)}$$

where θ_m is the value of θ corresponding to $y = L/2$ and defined by $\sin\theta_m = (L/2)/R_1$. The integration of (A4) gives

TABLE A1. Theoretical relative error (%) in the rain-rate estimate for a range of wind velocities. The wind is considered to blow (a) parallel or (b) perpendicular to the optical beam axis. The drops are supposed to be distributed in size according to a gamma formulation.

Wind velocity (m s^{-1})	Rain rate (mm h^{-1})		
	10	20	40
(a)			
2	−1.1	−0.9	−0.9
6	−3.5	−3.0	−2.7
10	−10.0	−7.6	−5.9
(b)			
2	−6.0	−7.3	−8.5
6	−7.3	−9.3	−11.4
10	−8.0	−11.4	−14.2

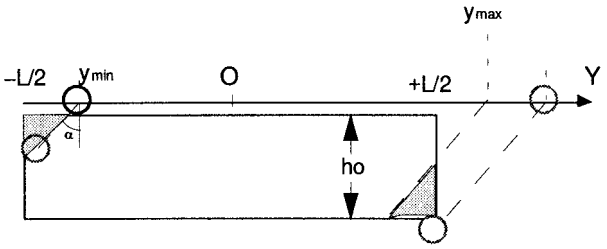

FIG. A2. Sketch of the particle trajectories in the cross section of the beam when the wind is perpendicular to the optical axis.

$$S_m = R_1\tan\alpha\left[R_1\theta_m + \frac{R_1}{2}\sin 2\theta_m - h_0\sin\theta_m\right]. \quad \text{(A5)}$$

Let α_0 be the value of the inclination angle α such that $\tan\alpha_0 = d/(D_2 - D_1)$, where d is the length of the first cylinder (see Fig. A1). When α becomes larger than α_0, the second cylinder of the box produces the shadow. The shadowed surface S_m then becomes

$$S_m = R_1\tan\alpha\left[R_2\theta_m + \frac{R_2}{2}\sin 2\theta_m - h_0\sin\theta_m\right] - Ld. \quad \text{(A6)}$$

The resulting rain-rate measurement error is obtained through numerical integration over the appropriate raindrop size distribution. The results are plotted versus the rain rate on Fig. 4 and numerical values are given in Table A1 (part a).

b. Wind normal to the optical axis

According to the notation detailed in Fig. A2, the drops with a trajectory tilt angle α, and an impact coordinate y between $-L/2$ and $L/2 + h_0\tan\alpha$ will be detected by the OSP. The sampling surface thus increases. On the other hand, the processing software rejects signals with duration less than $t_{\min}$ ($t_{\min} = 0.8$ m s^{-1}). This modifies the limiting detection coordinates along the y axis to

$$y_{\min} = -L/2 + \max(t_{\min}V_w + D/2,\ D\tan\alpha + D/2) \quad \text{(A7)}$$

and

$$y_{\max} = L/2 + h_0\tan\alpha - \max(t_{\min}V_w + D/2,\ D\tan\alpha + D/2). \quad \text{(A8)}$$

The resulting rain-rate measurement error versus the rain rate is also plotted in Fig. 4 and numerical values are given on Table A1 (part b).

REFERENCES

Augier, P., 1997: Contribution à l'étude et à la modélisation mécaniste-statistique de la distribution spatiale des apports d'eau sous un canon d'irrigation: Application à la caractérisation des effets du vent sur l'uniformité d'arrosage (Contribution to the study

and mechanical-statistical modelization of the water distributed from an irrigation gun: Application to characterize the effects of winds on water application uniformity). Ph.D. dissertation, Ecole Nationale du Génie Rural, des Eaux et des Forêts, Centre de Montpellier, France, 267 pp.

Beard, K. V., 1976: Terminal velocity and shape of cloud and precipitation drops aloft. *J. Atmos. Sci.,* **33,** 851–864.

Donnadieu, G., 1974: Étude des caractéristiques physiques et radioéléctriques de la pluie à l'aide d'un spectropluviométre photoélectrique. *J. Rech. Atmos.,* **8,** 253–266.

——, 1978: Mesure de la vitesse terminale des gouttes de pluie au sol à l'aide du spectromètre VIDIAZ. *J. Rech. Atmos.,* **12,** 245–249.

——, 1980: Comparison of results obtained with the VIDIAZ Spectro-Pluviometer and the Joss–Waldvogel rainfall disdrometer in a ''rain of a thundery type.'' *J. Appl. Meteor.,* **19,** 593–597.

——, G. Dubosclard, and S. Godard, 1969: Un pluviomètre photoélectrique pour la détermination simultanée des spectres dimensionnel et de vitesse de chute des gouttes de pluie. *J. Rech. Atmos.,* **4,** 37–46.

Folland, C. K., 1988: Numerical models of the raingauge exposure problem, field experiments and an improved collector design. *Quart. J. Roy. Meteor. Soc.,* **114,** 1485–1516.

Hauser, D., P. Amayenc, B. Nutten, and P. Waldteufel, 1984: A new optical instrument for simultaneous measurement of raindrop diameter and fall speed distributions. *J. Atmos. Oceanic Technol.,* **1,** 256–269.

Illingworth, A. J., and C. J. Stevens, 1987: An optical disdrometer for the measurement of raindrop size spectra in windy conditions. *J. Atmos. Oceanic Technol.,* **4,** 411–421.

Joss, J., and A. Waldvogel, 1967: Ein spektrograph für Niederschlagstropfen mit automatischer auswertung (A spectrograph for automatic measurement of raindrops). *Geofis. Pura Appl.,* **68,** 240–246.

Klaus, V., 1977: Étude d'un spectropluviomètre photoelectrique fournissant en temps réel des paramètres intégrés. Ph.D. dissertation, University of Paris VI, 96 pp. [Available from Université Paris VII, 4 Place Jussieu, 75252 Paris, Cedex 05, France.]

Knollenberg, R. G., 1970: The optical array: An alernative to scattering or extinction for airborne particle size determination. *J. Appl. Meteor.,* **9,** 86–103.

——, 1976: Three new instruments for cloud physics measurement: The 2D spectrometer, the forward scattering spectrometer probe and the active scattering aerosol spectrometer. *Proc. Conf. on Cloud Physics,* Boulder, CO, Amer. Meteor. Soc., 544–561.

Marshall, J. S., and W. M. Palmer, 1948: The distribution of raindrop with size. *J. Meteor.,* **5,** 165–166.

Picca, B., and G. Trouilhet, 1964: Un pluviogranulomètre photoélectrique (A photoelectric raindrop-size spectrometer). *J. Rech. Atmos.,* **7,** 184–188.

Pruppacher, H. R., and R. L. Pitter, 1971: A semi-empirical determination of the shape of cloud and rain drops. *J. Atmos. Sci.,* **28,** 86–94.

Rodda, J. C., 1967: The rainfall measurement problem. Preprints, *Conf. on Geochemistry, Precipitation, Evaporation, Soil-moisture, Hydrometry,* Bern, Switzerland, AIHS, 215–231.

Stow, C. D., and K. Jones, 1981: A self-evaluating disdrometer for the measurement of raindrop size and charge at the ground. *J. Appl. Meteor.,* **20,** 1160–1176.

Ulbrich, C. W., 1985: The effects of drop size distribution truncation on rainfall integral parameters and empirical relations. *J. Climate Appl. Meteor.,* **24,** 580–590.

Vastel, F., 1991: Station pluviométrique expérimentale DTG/IMG (An experimental pluviometric station). 36 pp. [Available from Université Montpellier II, ISIM, Place Eugène Bataillon, 34095 Montpellier, France.]

Wang, T.-I., K. B. Earnshaw, and R. S. Lawrence, 1979: Path-averaged measurements of rain rate and raindrop size distribution using a fast-response optical sensor. *J. Appl. Meteor.,* **18,** 654–660.